Proceedings of ASME Turbo Expo 2011
GT2011
June 6-10, 2011, Vancouver, British Columbia, Canada

GT2011-45866

NUMERICAL INVESTIGATIONS OF A SWIRL-STABILIZED PREMIXED FLAME AT ULTRA-WET CONDITIONS

Oliver Krüger[*], **Katharina Göckeler**, **Sebastian Göke**, **Christian Oliver Paschereit**
Institute of Fluid Dynamics and Technical Acoustics
Technical University Berlin, Müller-Breslau-Str. 8
D-10623 Berlin, Germany

Christophe Duwig
Laszlo Fuchs
Division of Fluid Mechanics
Department of Energy Sciences
Lund University, Box 118
SE-22100 Lund, Sweden

ABSTRACT

The present study focuses on the numerical investigation of a generic swirl-stabilized burner operated with methane at ultra-wet conditions. The burner is fed with a preheated homogeneous mixture formed by steam and air. As a set of operating conditions atmospheric pressure, inlet temperature of 673 K*, equivalence ratio of* 0.85 *and a steam content of* 30% *is applied.*

Large eddy simulations have been performed to investigate the flow features. In a first step the non-reacting flow field was investigated with water as working medium. Comparison with Particle Image Velocimetry (PIV) and Laser-Doppler Velocimetry (LDV) measurements conducted in a water tunnel facility showed that an excellent agreement within the experimental uncertainty is obtained for the flow field. A dominant frequency in the turbulent energy spectrum was identified, which corresponds to the motion associated with a precessing vortex core (PVC).

In order to investigate the reactive flow in a second step, a customized solver for handling low Mach number reacting flows based on an implicit LES approach was developed. As reaction mechanism a reduced 4 steps / 7 species global scheme was used. To compare the simulations qualitatively with a wet flame, OH chemiluminescence pictures serve as a reference. The simulations showed a more compact flame compared to the OH pictures. Nevertheless, the prolongation and position of the flame were found to be reasonable. The reduced mechanism captures the main effects, such as the reduction of the peak and mean temperatures. Furthermore, the presence of a PVC in the reacting flow could be determined and was not suppressed by heat-release.

NOMENCLATURE

A_0	Pre-exponential factor
b	Exponential factor of the Arrhenius equation
c	Concentration
c_p	Specific heat capacity
Co	Courant number
C_s	Smagorinsky constant
D_h	Hydraulic diameter
E_a	Activation energy
f	Frequency
F	Thickening factor
F	Volume force
h	Specific enthalpy
h_t	Total enthalpy
J	Laminar diffusive flux
Ka	Karlovitz number
m	Mass
m	Forward reaction order
p	Pressure
Pr	Prandtl number
r	Radial co-ordinate
Re	Reynolds number

[*]Corresponding author, o.krueger@tu-berlin.de

S_{th}	Theoretical swirl number
S_L	Laminar flame speed
t	Time
T	Temperature
u_0	Bulk velocity at burner exit
u_r	Radial velocity
u_t	Tangential velocity
u_x	Axial velocity
u'	Turbulent velocity fluctuation
$U_{s,t}$	Degree of unmixedness (s: spatial, t: temporal)
x	Axial co-ordinate
Y	Mass fraction
δ	Thermal thickness
Δ	Filter width
μ	Dynamic viscosity
μ_t	Eddy viscosity
Φ	Equivalence ratio
ρ	Density
τ	Characteristic time
τ_{ij}	Subgrid scale stress tensor
$\sigma_{s,t}$	Variance of concentration (s: spatial, t: temporal)
ω	Reaction rate
Ω	Air-steam ratio

INTRODUCTION

With the increasing concern about our environment, the control of the pollutant emissions becomes a more and more important focus in the design of modern gas turbine systems for power generation. In order to reduce harmful emissions, the current approach often is to design combustion devices operating under lean premixed conditions. This reduces the peak temperature and therefore, NOx emissions, but may lead to flame instabilities and higher UHC/CO emissions [1].

Another promising way is to add steam into the combustion process near stoichiometric conditions. Such Humidified Gas Turbines (HGT) offer the attractive possibility to increase the plant efficiency without the need of an additional steam turbine, as is the case for combined cycles. Adding steam directly into the combustion process increases the mass flow rate and the specific heat of the working fluid. Thus, a higher power output compared to a dry turbine can be achieved. Moreover, it reduces thermal NOx emissions significantly. In addition to the thermodynamical influence of the steam on the combustion process, an effect on the NOx formation pathways was observed. Even at constant adiabatic flame temperatures, NOx is reduced with increasing humidity [2, 3]. Beyond that, the exhaust heat can be used for steam generation which increases the cycle efficiency. Reducing the peak temperature even allows the operation with hydrogen-rich fuels due to the lower turbine inlet temperature. Therefore, combustion at ultra-wet conditions appears to be an interesting solution for application in industrial power plants. Different humidified gas turbine cycles have been discussed by Jonsson and Yan [4].

The aim of the current study is to compare the numerical methods and models under ultra-wet conditions with experimental data. In a future step, the aim is to improve the combustion process to be suitable for industry application by changing the flow field. Thus, this work is a preliminary but mandatory step to address problematic behavior arising in the simulations to ensure portability on more complex situations. Especially the turbulent combustion is a complex topic which involves non-linear multi-scale phenomena. For the combustion process fuel, oxidant and heat is needed. At high Reynolds numbers the coexistence of these three factors highly depends on the turbulent micro-mixing. Consequently, the flame location is unsteady in nature and very sensitive to perturbations. The high sensitivity of the flame stresses the importance and the need for a better understanding of the flame dynamics and stabilization.

Investigations on humidified combustion processes have been published by Bianco [5] and Guo [6], but only up to a water-air ratio of 5%. In the current study a steam content of 30% is investigated. The steam content $\Omega = \dot{m}_{steam}/\dot{m}_{air}$ is defined as the ratio of the mass flow of steam $\dot{m}_{steam}$ to the mass flow rate of air $\dot{m}_{air}$.

In order to analyze the flame behavior under wet conditions, a generic swirl burner fed with methane and humidified air has been used for Large Eddy Simulations (LES) to predict the velocity field, flame shape, and temperatures. The simulations are compared to experimental results.

The numerical simulation of the isothermal swirling flow is an important tool to assist experiments to gain deep understanding of the fundamental flow physics. Especially the coherent structures and the motion of the precessing vortex core (PVC) were captured accurately. Therefore, a simulation of the non-reacting flow with water as fluid was conducted and validated against measurements in a water tunnel facility.

In order to handle the wet combustion, a customized solver based on an implicit LES formulation for handling reacting flows at low Mach numbers was developed. As reaction mechanism a reduced 4 steps / 7 species global scheme by Lindstedt and Jones [7] was used. This enables to resolve more details of the flame structure but avoids the stiffness and CPU burden of a detailed mechanism.

Firstly, the investigated geometry and the experimental and numerical techniques are presented. Secondly, the flow is discussed using averaged and RMS velocity fields obtained from LDV, PIV and LES for the non-reacting case. Afterwards the simulation of the reacting flow is compared to OH chemiluminescence recordings. Finally, the results are summarized and conclusions are drawn.

INVESTIGATED CONFIGURATION

The simulations have been carried out on a cylindrical computational domain with an attached swirl generator, as shown in Figure 1. The domain is adopted from the experimental set-up. Only the length of the combustion chamber was truncated, due to limited computational resources. The characteristic length and velocity were chosen to be the hydraulic diameter $D_h = 27.5\,\mathrm{mm}$ and the mean bulk velocity u_0 at the burner exit. Thus, a characteristic timescale $\tau = {}^{D_h}/_{u_0}$ can be defined for normalization.

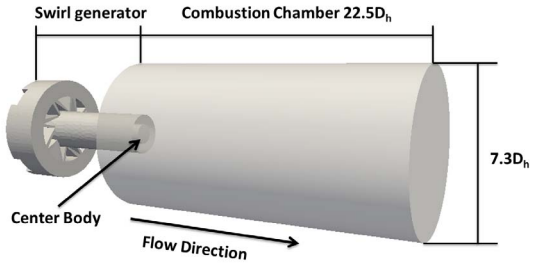

FIGURE 1. SCHEMATIC OF THE COMPUTATIONAL DOMAIN.

The MOVABLE BLOCK BURNER used in this investigation is based on a design developed by the INTERNATIONAL FLAME RESEARCH FOUNDATION, IFRF [8]. It consists of eight movable and eight fixed blocks, which are placed alternately, as shown in Figure 2. Due to simultaneous rotation of the movable blocks about the symmetry axis, the oblique passages are opened while the non-oblique parts are narrowed and vice versa. This yields an increase or reduction of the swirl intensity. The swirl number can be derived by the geometry [9] and varied between 0 and 2. Air and steam are premixed before entering the swirl generator. Fuel is injected directly at the bottom plate of the swirl generator through 16 holes. The fuel mixes with the swirling flow in the annular passage to the combustion chamber.

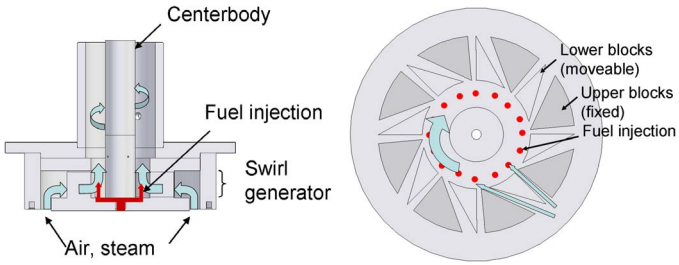

(a) Generic Burner (b) Swirl Generator

FIGURE 2. SECTIONAL VIEW OF THE GENERIC BURNER AND THE SWIRL GENERATOR.

EXPERIMENTAL TECHNIQUES

The non-reacting flow experiments were conducted in a water tunnel under atmospheric conditions. An unscaled Plexiglas model of the burner allowed optical access for the application of laser diagnostics. As non-intrusive techniques Laser Doppler Velocimetry (LDV) as well as Particle Image Velocimetry (PIV) were applied. The setup is sketched in Figure 3. For the LDV a two-component backscatter LDV system by DANTEC DYNAMICS was used to measure the tangential and axial velocities at various axial positions. For both the PIV and the LDV measurements silver coated hollow glass spheres with a diameter of $15\,\mu\mathrm{m}$ were employed. A three-dimensional traverse system ensured the positioning of the measurement volume. Distinct refraction indexes of air, glass and water were taken into account. Depending on the position a data rate of 50 Hz to 350 Hz was achieved. The PIV measurements were performed using a Nd:YAG pulse laser and a PCO Sensicam. The experimental set-up and equipment was discussed in detail in [10] and [3].

In order to enable a comparison between the water tunnel experiments and the gas-fired tests the Reynolds number was kept constant. The tested air-steam mass flow rate was $180\,{}^{\mathrm{kg}}/_{\mathrm{h}}$, which corresponds to a Reynolds number of $Re = 33,000$ for a steam content of $\Omega = 30\%$ and a preheat temperature of $T = 673\,\mathrm{K}$. The

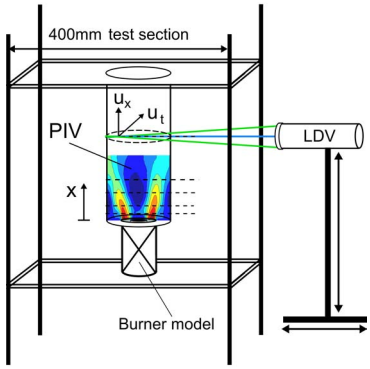

FIGURE 3. SCHEMATIC OF THE SETUP FOR FLOW MEASUREMENTS.

gas-fired measurements were conducted in a test rig under atmospheric conditions. As fuel natural gas was used. The air was preheated and mixed with overheated steam, which resulted in an inlet temperature of $T = 673\,\mathrm{K}$. In previous investigations the mixing quality of the air-steam-fuel mixture was measured [3]. The spatial and temporal degree of unmixedness is described as $U_{s,t} = \sigma^2_{s,t}/\bar{c}(1-\bar{c})$, where $\sigma_{s,t}$ is the temporal (index t) or spatial (index s) variance of concentration fluctuations and $\bar{c}$ is the mean molar fuel concentration. It was observed that the spatial and temporal degree of unmixedness was in the order of $\approx 10^{-4}$. Thus, the air-steam-fuel mixture can be regarded as technically

TABLE 1. Operating Conditions

Condition	Case 1	Case 2
Fluid	Water	Air/ Steam/ Methane
Inlet Velocity u_{in}	0.6 m/s	35 m/s
Bulk Velocity u_0	1.3 m/s	64 m/s
Inlet Temperature T_{in}	291 K	673 K
Pressure p	101,325 Pa	101,325 Pa
Reynolds number Re	33,000	33,000
Steam Content Ω	-	30%
Equivalence Ratio Φ	-	0.85

premixed which has been taken into account for the simulation by supplying the inlet directly with premixed gases. Therefore the methane injection system and the mixing process were not regarded. The flame position was assessed by recording its OH chemiluminescence using an ICCD camera. In order to recover the radial intensity distribution the images were decomposed applying an Abel deconvolution according to [11].

As mentioned above for the simulations and the experiments the same geometry was used. The combustion chamber was a cylindrical silica glass with a diameter of 0.2 m. This results in an area expansion ratio of 17.5. The swirl number was adjusted to $S_{th} = 0.7$ to assure a vortex breakdown in the combustion chamber. The operation conditions are summarized in Table 1.

NUMERICAL METHODS

The motion of a fluid is described by basic equations as the conservation of momentum, mass, species and energy. In LES a "low-pass" filter is applied to the dependent variables so that the filtered equations only describe the larger turbulent fluctuations [12, 13]. The Favre averaged filtered equations are described as follows:

Mass:

$$\frac{\partial \overline{\rho}}{\partial t} + \frac{\partial \overline{\rho}\tilde{u}_j}{\partial x_j} = 0\,. \tag{1}$$

Momentum $(i = 1,2,3)$**:**

$$\frac{\partial \overline{\rho}\tilde{u}_i}{\partial t} + \frac{\partial (\overline{\rho}\tilde{u}_j\tilde{u}_i)}{\partial x_j} = -\frac{\partial}{\partial x_j}\left[\overline{\rho}\left(\widetilde{u_i u_j} - \tilde{u}_i\tilde{u}_j\right)\right] - \frac{\partial \overline{p}}{\partial x_i} + \frac{\partial \overline{\tau}_{ij}}{\partial x_j} + \overline{F_i}\,, \tag{2}$$

where u_i is the velocity component, ρ the density, p the pressure, μ the dynamic viscosity, F_i a volume force and τ_{ij} is an unclosed term, usually denoted as the subgrid scale stress tensor. The superscripts $-$ and $\sim$ refers to LES filtered quantities rather than ensemble means. The mass conservation equation for chemical species k is described as follows:

$$\frac{\partial \overline{\rho}\tilde{Y}_k}{\partial t} + \frac{\partial}{\partial x_i}\left(\overline{\rho}\tilde{u}_i\tilde{Y}_k\right) = \frac{\partial}{\partial x_i}\left[\overline{J_i^k Y_k} - \overline{\rho}\left(\widetilde{u_i Y_k} - \tilde{u}_i\tilde{Y}_k\right)\right] + \overline{\dot{\omega}_k}\,, \tag{3}$$

where Y_k is the mass fraction of the species k, $\dot{\omega}_k$ is the reaction rate and J_i^k is the i-component of the laminar diffusive flux of species k. For the conservation of the enthalpy the following equation is used, where a low Mach assumption is regarded:

$$\frac{\partial \overline{\rho}\tilde{h}_t}{\partial t} + \frac{\partial \overline{\rho}\tilde{u}_i\tilde{h}_t}{\partial x_i} = \frac{\partial}{\partial x_i}\left(\frac{(\mu_t + \mu)}{Pr}\frac{\partial \tilde{h}_t}{\partial x_i}\right)\,, \tag{4}$$

where h_t is the total enthalpy, μ the dynamic viscosity of the fluid, μ_t is the eddy viscosity and $Pr = 0.7$ the Prandtl number. The total enthalpy $h_t = h + {}^{u_i u_j}/_2$ can be described by the specific enthalpy h.

The filtering can be described by a linear function which is assumed to be commutative with temporal and spatial derivatives. The filtering is not commutative for non-linear terms. Therefore, these terms cannot be expressed in terms of the filtered variables and hence they are gathered on the right-hand side. These terms are collectively called the subgrid scale (SGS) term. In this study the SGS term is modeled by the classical Smagorinsky approach [14]. In this approach the unresolved stress tensor $\tau_{ij} = \overline{\rho}\widetilde{u_i u_j} - \overline{\rho}\tilde{u}_i\tilde{u}_j$ is modeled using the BOUSSINESQ hypothesis, in which the effect of the unresolved turbulence on the large-scale flow is modeled as an increase in the viscosity. The filter length scale is the cubic root of the local grid cell volume. The Smagorinsky constant C_s was set to $C_s = 0.1683$.

All the simulations have been carried out using the open-source solver platform OpenFOAM. For the non-reacting cases the standard framework was used. In order to handle the wet combustion, a customized solver for low Mach number reacting flows was developed. By doing so, the density is a function of the mixture composition and temperature only. For both cases the pressure velocity coupling is performed using the PISO algorithm as described by [15, 16], ensuring that continuity is satisfied. Second order differencing is used for all spatial derivatives except for the convective terms in the enthalpy and the mass fraction equations. These are treated using a second order accurate total-variation-diminishing (TVD) scheme for avoiding unphysical over-shoots. Time derivatives are treated using a second order upwind scheme and time integration is done implicitly in a sequential manner.

TABLE 2. J& L Four-step global kinetic mechanism for humidified methane oxidation

Reaction	A_0	b	E_a
Unit	$(-)$	$(-)$	$(\frac{cal}{mol})$
$[CH_4]^{0.5} + [\frac{1}{2} O_2]^{1.25} \Rightarrow CO + 2H_2$	$1.446 \cdot 10^{13}$	0.0	$30 \cdot 10^3$
$[H_2]^{0.25} + [\frac{1}{2} O_2]^{1.5} \Rightarrow H_2O$	$0.3623 \cdot 10^{18}$	-1.0	$40 \cdot 10^3$
$[CH_4]^1 + [H_2O]^1 \Rightarrow CO + 3H_2$	$0.9000 \cdot 10^{11}$	0.0	$30 \cdot 10^3$
$[CO]^1 + [H_2O]^1 = CO_2 + H_2$	$0.8100 \cdot 10^{12}$	0.0	$20 \cdot 10^3$
$k = A_0 T^b \exp\left(-\frac{E_a}{R \cdot T}\right)$; $[\,]^m$:m = forward reaction order			

TABLE 3. A freely propagating flame computed with J&L wet and GRI3.0. Operating conditions: $\Phi = 0.85$, $\Omega = 0.3$, perfectly premixed and preheated to $T_{in} = 673\,\mathrm{K}$

Quantity	J&L wet	GRI3.0
Flame speed SL (m/s)	0.336	0.347
Thermal thickness (m)	0.00123	0.00107

Dirichlet boundary conditions are enforced at the inlet for all variables except pressure which uses a zero gradient condition (Neumann). Similarly, the out flow is treated using zero gradient for all variables except for pressure for which a Dirichlet boundary condition was used. Non slip walls (zero velocity) are used with zero gradient for the other variables, hence assuming an adiabatic combustor.

REACTION MECHANISM

Incorporating combustion chemistry into LES involves finding a suitable reaction mechanism and solving the filtered species equations. Appropriate reaction mechanisms may involve tens or hundreds of species with hundreds or thousands of reaction steps, but are often drastically reduced to avoid solving a large system of stiffly coupled equations. Presently, we use a 4 steps / 7 species global scheme enabling to resolve some details of the flame structure (hydrogen and carbon monoxide peak) but avoiding the stiffness and CPU burden of a detailed mechanism. The chemical scheme is based on the work by Lindstedt and Jones [7]. However, they considered different operating conditions and therefore the pre-exponential coefficients were altered to fit better the present operating conditions. In other words, the pre-exponential coefficients were modified so that the scheme fits the freely propagating flame data computed with a detailed chemical mechanism, namely GRI 3.0 [17]. The Linstedt and Jones scheme is given in Table 2: The first three reactions account for the methane and hydrogen oxidation and are irreversible. The last reaction is the reversible water gas shift reaction. The reaction rates $\dot{\omega}$ are calculated by the Arrhenius equation. The coefficients of the Arrhenius equation A_0, b and the activation energy are listed in Table 2. Table 3 shows the good agreement between the modified Lindstedt and Jones scheme (referred as J&L wet) and the GRI data. In addition, Figure 4 shows the temperature profile for the corresponding freely propagating flames. The 4-steps scheme fits closely the GRI 3.0 profile up to $T \approx 1650\,\mathrm{K}$ and departs in the post-flame zone. In particular, the CO oxidation layer length is under-estimated by J&L wet.

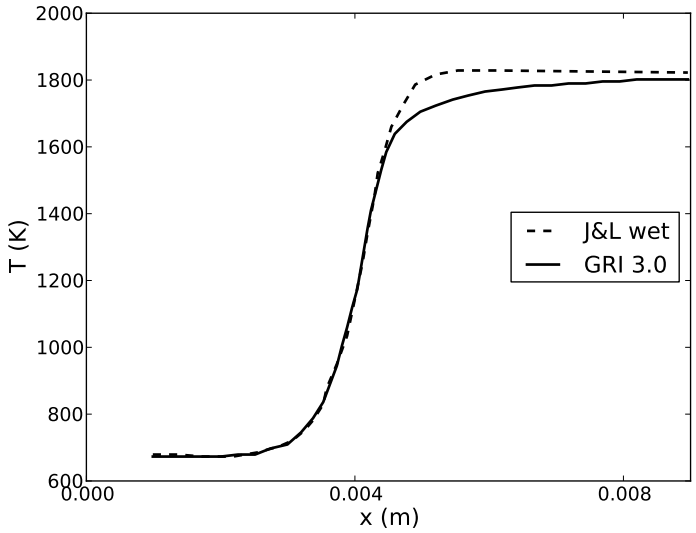

FIGURE 4. TEMPERATURE PROFILE FOR A ONE DIMENSIONAL FREELY PROPAGATING FLAME COMPUTED WITH J&L WET AND GRI 3.0. OPERATING CONDITIONS: $\Phi = 0.85$, $\Omega = 0.3$, PERFECTLY PREMIXED AND PREHEATED TO $T_{in} = 673\,\mathrm{K}$

An additional modeling issue lies in the filtered species equations which contain the filtered reaction rates $\overline{\dot{\omega}}$. The reaction rates are non-linear functions of species concentration and temperature. Different avenues have been used for modeling of the filtered reaction rate, starting by extending Reynolds Averaged Navier-Stokes (RANS) combustion models to LES applications. Recently modern methods have been proposed that were specifically designed for the LES framework [18].

Examples of such methods include (i) Implicit LES (ILES), [19–22], (ii) Thickened Flame Models (TFM) [18, 23], (iii) Lin-

ear Eddy Models (LEM) with embedded 1D grids [24], (iv) Flamelet Models (FM) [25–28], (v) Eddy Dissipation Concept (EDC) [29], (vi) Partially Stirred Reactor (PaSR) [19] and (vii) Filtered Density Function (FDF) models [20,30]. If the methods (iv-vi) have a counter-part in the RANS framework, the methods (i-iii) are solely valid for LES applications.

The investigated flame in the present paper is characterized by a relatively high Karlovitz number as a large amount of steam is added to the reactants, which spreads the heat release peak. The Karlovitz number can be calculated by

$$Ka \sim \left(\frac{u'}{S_L}\right)^{\frac{3}{2}} \left(\frac{D_h}{\delta}\right)^{-\frac{1}{2}} \approx 180\,, \tag{5}$$

where u' is the velocity fluctuation, S_L the laminar flame velocity and δ the flame thickness. The thermal thickness δ and the laminar flame velocity are listed in Table 3. With such a high Karlovitz number the flame lies well in the distributed reaction regime. Therefore, the flame is definitely subject to strong finite rate chemistry effects and suitable candidates for resolving this effect are ILES, TFM, LEM, EDC, PaSR and FDF. LEM and transported-FDF are very CPU expensive techniques when used with LES, while presumed-FDF and ILES keep the CPU cost at reasonable levels. EDC and PaSR have intermediate CPU cost, though potentially important when dealing with complex burner geometries. The present study focus on using ILES which has the attractive feature of handling complex chemistry naturally and with reasonable extra cost. For species j, the ILES (also referred sometimes as Monotonically Integrated LES - MILES) closure [19–22] gives:

$$\overline{\dot{\omega}_j\left(Y_i,T\right)} = \dot{\omega}_j\left(\tilde{Y}_i,\tilde{T}\right)\,, \tag{6}$$

where the reaction rate is obtained from an Arrhenius expression. Equation (6) would fail in the RANS framework, but is valid for laminar flow simulation and direct numerical simulation (DNS). The validity of Equation (6) with LES depends on the relative grid resolution and also on the subgrid physics. Although using a typical LES-grid, far from DNS, Equation 6 was shown to approximate reasonably well the reaction rate as reported [19–22]. These studies suggest that ILES is an eligible approach for combustion simulation and that it may perform equally well than other closures.

The assumption leading to ILES correspond to a perfectly stirred reactor with a homogeneous subgrid concentration and temperature. Therefore, a very intense subgrid mixing is required to ensure that the filter box, or LES grid cell, is homogeneous. From a balance perspective, it implies that the subgrid mixing acts faster than any chemical reaction. An alternative measure is the thickening factor F used in the TFM. The factor F is usually computed in order to be able to resolve the flame front on $3-5$ grid points, $F \sim 3\Delta/\delta_L \approx 0.6$. Usually F is less sensitive than the local Damköhler number Da as it does not account for the subgrid stirring, though the ILES domain of validity corresponds to F close or below 1. $F \approx 0.6$ indicates that the present flame falls well into the domain of validity of ILES and the reaction brush is indeed resolved on the LES grid.

The computations are run with a Reynolds number of $Re \approx 33,000$. A grid with 2.3 millions computational was used. The grid size was calculated by the autocorrelation of the velocity fluctuations for one point in the shear layer to be of the order of the Taylor turbulent length scale ($\approx 0.015 D_h$). Thus, the smallest resolved scales are in the inertial range of the turbulent spectrum and the grid is suitable for performing LES.

RESULTS AND DISCUSSION

Non-Reacting Flow Field

The performed LES computation run with a constant time step of $\Delta t = 10^{-5}$ s. The maximum Courant number was kept below $Co \leq 0.27$. The typical Courant number in the shear layer was $Co = 0.08$. The operating conditions for the non-reacting case is listed in Table 1.The result was time averaged over two physical seconds after reaching a statistically steady state and showed a symmetrically averaged velocity field.

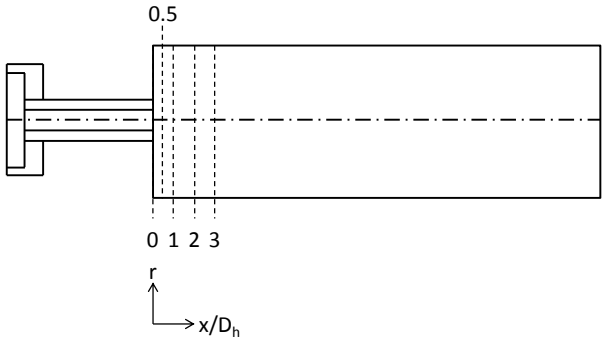

FIGURE 5. VIEW OF THE DIFFERENT AXIAL LOCATIONS FOR THE FURTHER DISCUSSION. THE BURNER EXIT IS LOCATED AT $x/D_h = 0$.

For the following discussion, velocity plots are shown at different axial positions. These positions are presented in Figure 5. The origin ($x/D_h = 0$) is located in the plane at the burner exit and all co-ordinates are normalized by the hydraulic diameter D_h. Figure 6 gives a comparison of the measured and simulated axial mean flow field at different axial positions. Near the burner exit a recirculation zone establishes due to vortex break down downstream of the sudden expansion. The LES over predicts

the negative velocity near the burner exit ($x/D_h = 0.5$) slightly in comparison to the measurements. This effect diminishes further downstream. High velocity gradients are reached in the shear layer between the recirculation zone and the surrounding swirling flow. The computation and the measurements show a very good agreement.

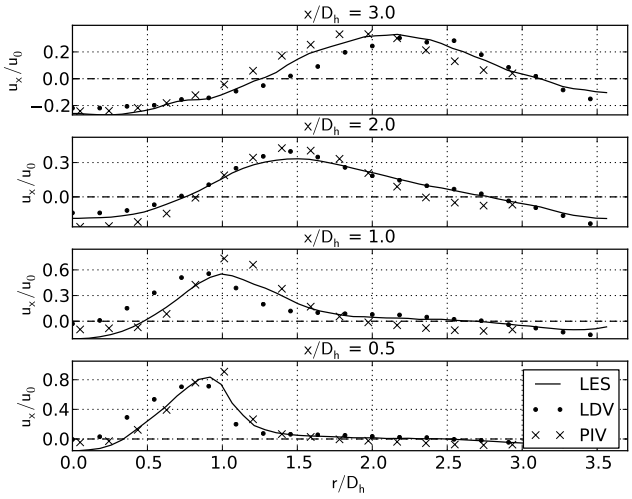

FIGURE 6. STREAM WISE VELOCITY u_x/u_0 PROFILES AT 4 DIFFERENT AXIAL LOCATIONS DOWNSTREAM OF THE BURNER EXIT ($x/D_h = 0$) FOR THE NON-REACTING CASE.

The radial- (u_r) and tangential velocities (u_t) are shown in Figure 7 at two different axial positions. Different techniques were applied measuring radial and tangential velocities. At both positions the tangential velocities of the LDV and the LES match at near the wall; in the recirculation zone some discrepancies appear. The radial velocities show a good agreement, even if the aberration is higher compared to the tangential velocities.

The RMS values of the velocity fluctuations are also compared and presented in Figure 8.

The LES shows a close agreement to PIV and LDV. This is indicating that the LES tool captures the fluctuations both qualitatively and quantitatively. Small discrepancies in the inner recirculation zone are seen. Nevertheless, the LES is able to predict the flow field and most notably the vortex break down correctly.

The LES captures the fluctuation levels well indicating the coherent structures are accurately resolved. The existence of coherent structures can be obtained from the energy time spectrum of the random-fluctuations. The energy spectrum describes the energy cascade, thus the energy transfer between large scales and small scales. For a single point located near the burner exit ($x/D_h = 1$) on the symmetry axis the spectrum is plotted in Figure 9. The computations are able to predict the height and the

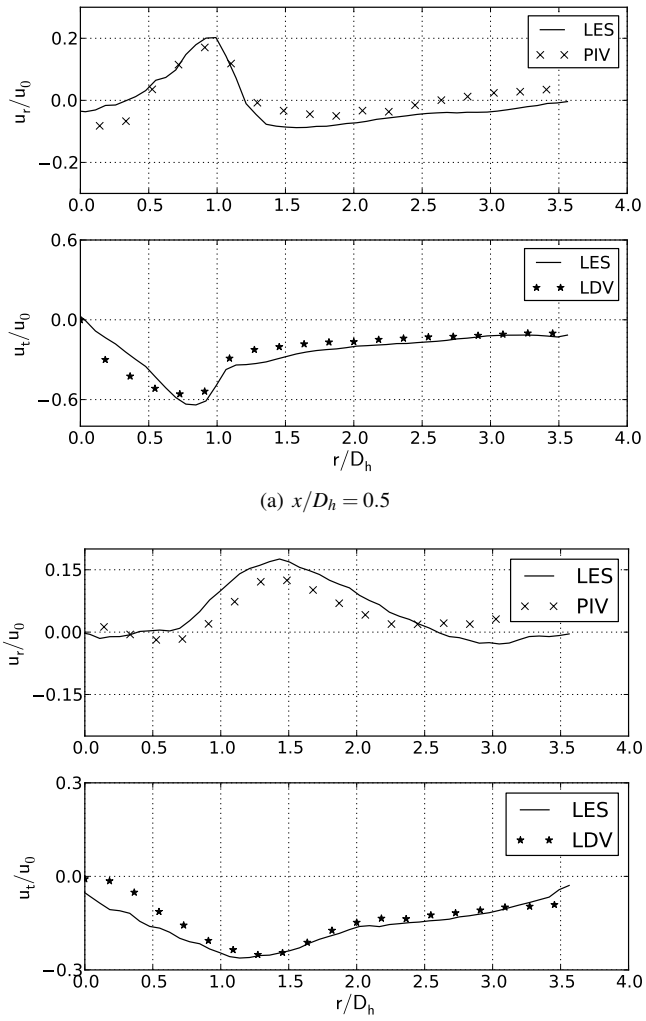

(a) $x/D_h = 0.5$

(b) $x/D_h = 2.0$

FIGURE 7. RADIAL (u_r/u_0) AND TANGENTIAL (u_t/u_0) VELOCITY PROFILES AT THE AXIAL LOCATION $x/D_h = 0.5$ (TOP) AND $x/D_h = 2.0$ (BOTTOM) DOWNSTREAM OF THE BURNER EXIT ($x/D_h = 0$) FOR THE NON-REACTING CASE.

characteristic of the inertial subrange reasonably as can be seen by comparison with the Kolmogorov $-5/3$ power law. Moreover, a dominant frequency of $f = 9.2\,\text{Hz}$ is seen which implies the existence of a coherent structure as investigated in [31]. Using a similar configuration, it was observed in [31] that the dominant frequency is related to the swirling motion of a coherent structure.

Coherent structures are associated with local minima of the pressure field as shown in [32, 33]. In Figure 10 this structure is shown through an iso-surface of the pressure. The images show an instantaneous snapshot of the structure oscillating around the center body. The time step between the first and the last mo-

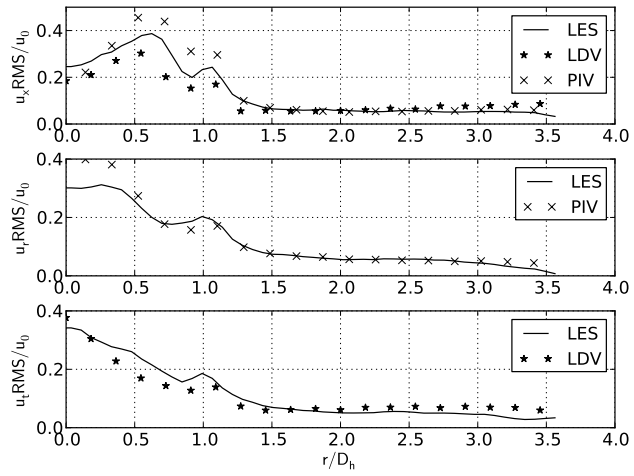

(a) $x/D_h = 0.5$

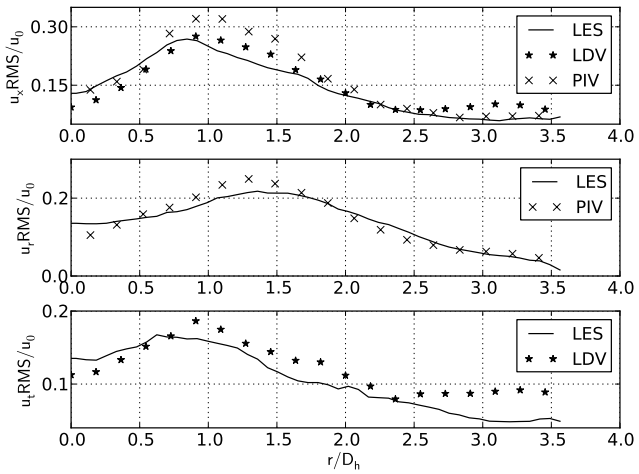

(b) $x/D_h = 2.0$

FIGURE 8. RMS OF THE FLUCTUATIONS OF THE STREAM WISE (u_xRMS/u_0), RADIAL (u_rRMS/u_0) AND TANGENTIAL (u_tRMS/u_0) VELOCITY COMPONENTS AT THE AXIAL LOCATION $x/D_h = 0.5$ (TOP) AND $x/D_h = 2.0$ (BOTTOM) DOWNSTREAM OF THE BURNER EXIT ($x/D_h = 0$) FOR THE NON-REACTING CASE.

ment is equal to a half-period of the dominant frequency. Due to its helical characteristic it can be denoted as a precessing vortex core (PVC). García-Villalba [31] described that the motion of the PVC can be decomposed into components. The first is a rotation of the vortex core around the symmetry axis and the second is a spinning of the vortex around its own axis. The latter one could not be observed, due to the fact, that the pressure minimum is not constant over different time steps.

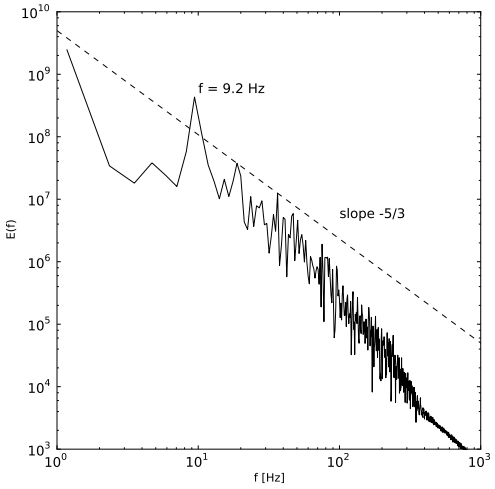

FIGURE 9. TURBULENT KINETIC ENERGY SPECTRUM DETERMINED FOR A SINGLE POINT LOCATED WITHIN THE RECIRCULATION ZONE ON THE STREAM WISE SYMMETRY AXIS ONE DIAMETER ($x/D_h = 1$) DOWNSTREAM OF THE BURNER EXIT.

Reacting Flow Field

In the results of the reactive computations are discussed. The performed LES computation run with an adjustable time step to keep the maximum Courant number below $Co = 0.2$. This resulted in an averaged time step of 10^{-6} s. As a set of operating conditions atmospheric pressure, inlet temperature of $T_{in} = 673$ K, equivalence ratio of $\Phi = 0.85$ and a steam content of $\Omega = 30\%$ was applied. Moreover, fuel and the air-steam-flow enter the combustion chamber as a homogeneous mixture. Investigations on the comparison between the wet and the dry case was reported previously [3] in terms of emissions and extinction limits and is not presented here.

Figure 11 shows the instantaneous temperature and CO concentration field as predicted by the LES computation. As can be seen, the flame is irregular with steep gradients. Close to the burner exit, the flame is weakly wrinkled. Further downstream, the flame pattern changes, exhibiting larger wrinkles. These wrinkles can be described as large eddies in circumferential direction. The adiabatic temperature of the air-steam-methane mixture is with $T = 1812$ K significantly lower than the adiabatic flame temperature for the same conditions but without steam with $T_{dry} = 2292$ K. As proposed before, the addition of steam increases the specific heat and therefore the peak temperature. The increase of the specific heat capacity can be calculated for an ideal mixture with $c_p(T) = \Sigma_i(Y_i \cdot c_{p,i}(T))$. For the perfectly premixed air-steam-methane composition at $T = 673$ K and atmospheric conditions, the specific heat capacity calculates for the dry case to $c_{p,dry} = 1.117 \frac{\text{kJ}}{kg/\text{K}}$ and for the wet case to $c_{p,wet} = 1.328 \frac{\text{kJ}}{kg/\text{K}}$. The CO concentration reaches its maximum

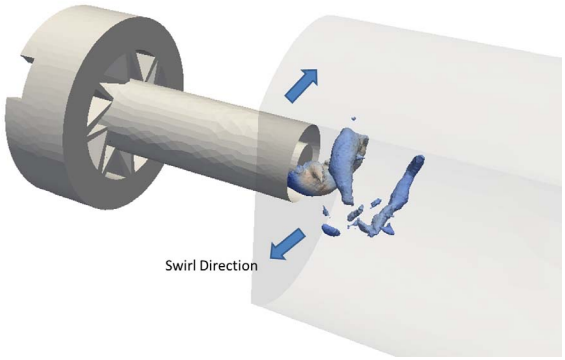

(a) Pressure isosurface at $t/\tau = 152$

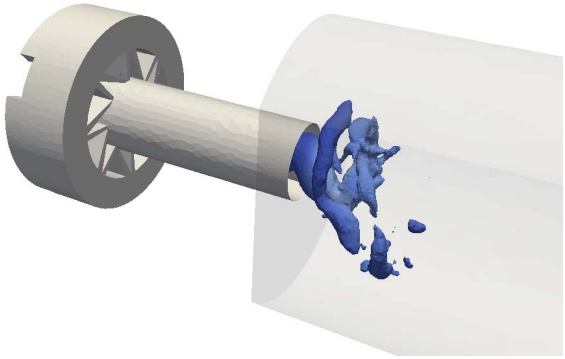

(b) Pressure isosurface at $t/\tau = 155.5$

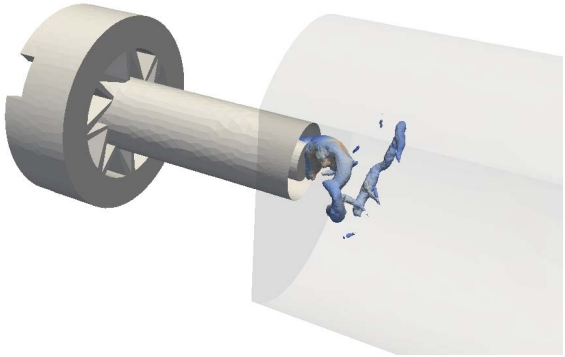

(c) Pressure isosurface at $t/\tau = 157$

FIGURE 10. VISUALIZATION OF THE HALF-PERIOD ROTATION OF THE COHERENT STRUCTURE FOR THE NON-REACTING CASE. STRUCTURE IS REPRESENTED BY A ISO-PRESSURE CONTOUR. THE STRUCTURE IS COLORED WITH THE TURBULENT FLUCTUATION IN STREAM WISE DIRECTION ($u_x RMS$).

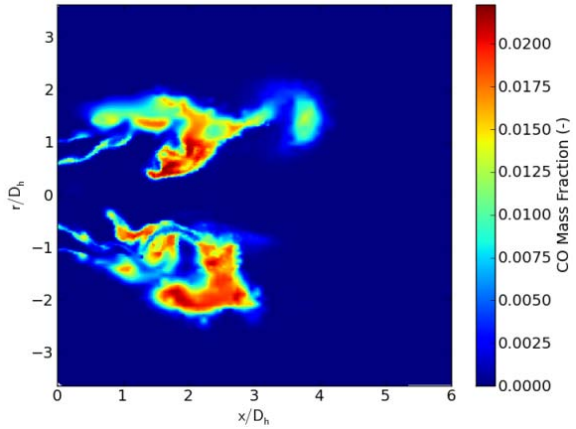

(a) Mass Fraction of CO

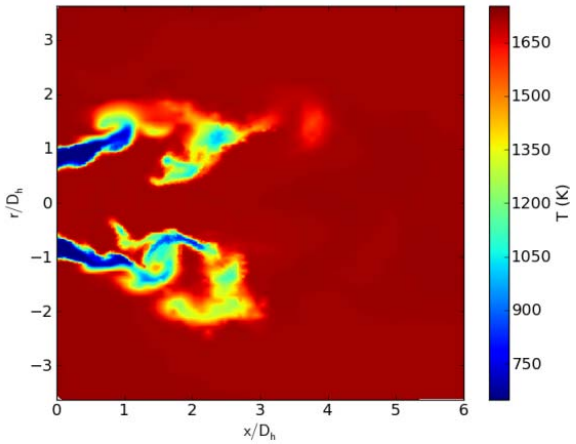

(b) Temperature field

FIGURE 11. SLICES IN STREAM WISE DIRECTION SHOWING INSTANTANEOUS FIELDS FOR THE REACTING CASE ($\Phi = 0.85$, $\Omega = 0.3$, $T_{in} = 673\,\mathrm{K}$). THE BURNER EXIT IS LOCATED AT $x/D_h = 0$. TOP: INSTANTANEOUS CO CONCENTRATION (MASS FRACTION), BOTTOM: INSTANTANEOUS TEMPERATURE FIELD

at $\approx 1300\,\mathrm{K}$ within the flame zone. Figure 12 shows a slice through the combustion chamber at the stream wise position $x/D_h = 2.3$. As can be seen, the CO concentration has a ring shape and no CO is found within the inner recirculation zone. The fact that no combustion process takes place inside of the ring shape can be attributed to the recirculating flow of the inner recirculation zone. Figure 12 shows the axial velocity at axial position $x/D_h = 2.3$. The recirculating flow supplies the flame with reaction products, mainly with H_2O and CO_2 which pushes the flame into the shear layer.

The flame is approximately represented by the concentration of active OH radicals. An OH-chemiluminescence image of the flame serves for a qualitative comparison with the computation. This image was transformed by an Abel inversion to give a view of the flame in a slice without losses induced by the integration through the line of sight. So, the result of the inversion is an image of the reaction layer. The algorithm for the inversion is based on the relationship to the Fourier and Hankel transforms and was presented by Jaffe [11]. The reduced mechanism, as listed in Ta-

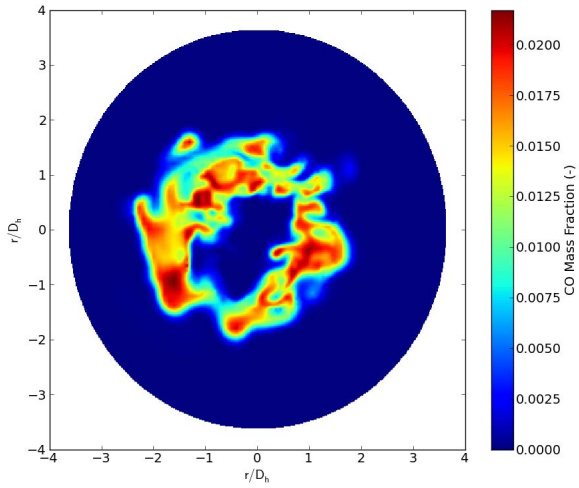

(a) CO Mass Fraction

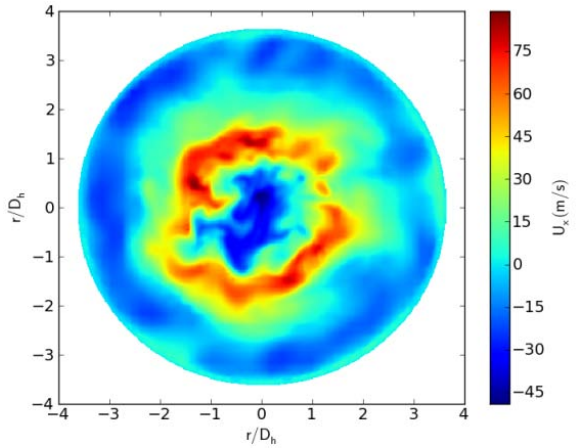

(b) Axial Velocity Field

FIGURE 12. SLICES OF THE INSTANTANEOUS REACTING FIELD ($\Phi = 0.85$, $\Omega = 0.3$, $T_{in} = 673\,\mathrm{K}$) AT THE AXIAL POSITION $x/D_h = 2.3$. TOP: CO CONCENTRATION (MASS FRACTION), BOTTOM: STREAM WISE VELOCITY COMPONENT

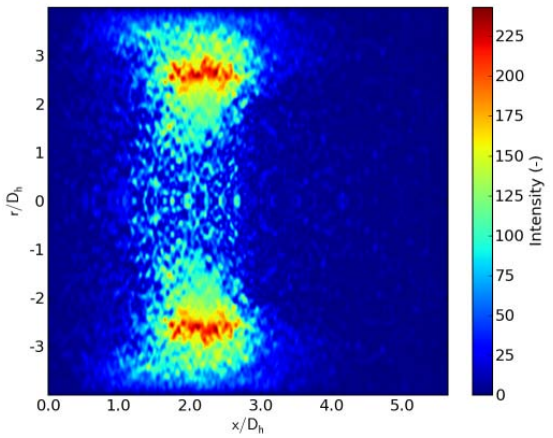

(a) Representation of the processed Abel Inversion of OH-chemiluminescene measurements

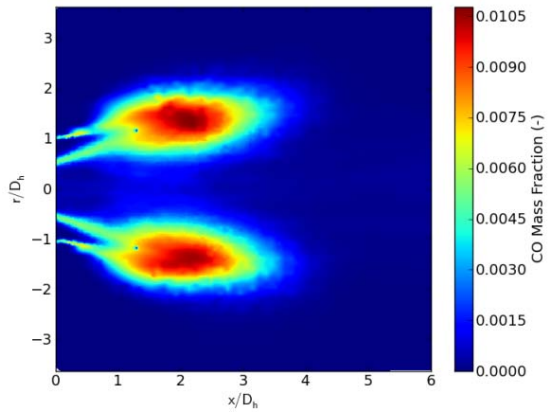

(b) Temporal average of the CO concentration

FIGURE 13. COMPARISON OF THE REACTING LES ($\Phi = 0.85$, $\Omega = 0.3$, $T_{in} = 673\,\mathrm{K}$) AND THE MEASUREMENT. TOP: PROCESSED ABEL INVERSION OF OH-CHEMILUMINESCENE MEASUREMENTS, BOTTOM: SLICE OF THE MEAN CO CONCENTRATION (MASS FRACTION) OF THE LES

ble 2, does not take the OH formation into account, but the CO concentration can be used as an indicator for the flame characteristics. Figure 13 shows the Abel deconvoluted image of the OH radicals as well as the mean CO concentration of the LES. As shown in previous investigations [10] the flame has a v-type shape and is stabilized in the inner shear layer. It was also shown that the flame shape changes by adding steam to the combustion process, as it can be observed in the simulation. As can be seen in Figure 13 the reaction zone extends further downstream. The main reaction zone is located closer to the wall. The LES shows a more compact reactive zone than the OH-image and a slightly axial offset, which is a consequence of the reduced mechanism. The chemistry predicts 'shorter' CO oxidation zones. Nevertheless, the dimension of the main reaction zone and the drop-shape seems to be reasonably predicted. Other experimental methods for quantitatively comparisons have not been employed yet, but they are in the focus for upcoming investigations.

In the cold flow investigations a coherent structure was found. This structure was attached to the center body and was rotating around it. The basic question is if the heat release suppresses the formation of a coherent structure. This question can be denied, due to the fact, that for the reacting case a coherent structure could be detected. This structure is represented by the Q-criterion as shown in Figure 14 and the structure is highlighted with the axial velocity. The definition of the Q-criterion is presented in [34]. The criterion shows small vortex tubes, which are embedded in the PVC. Some tubes are orientated circumferen-

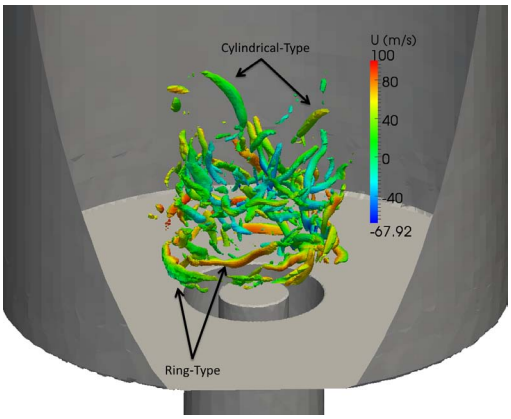

(a)

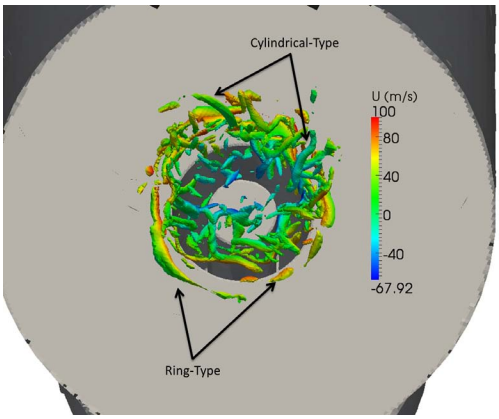

(b)

FIGURE 14. VISUALIZATION OF THE COHERENT STRUCTURES BY USING THE Q-CRITERION FOR THE REACTING CASE ($\Phi = 0.85$, $\Omega = 0.3$, $T_{in} = 673\,\mathrm{K}$) FOR TWO DIFFERENT PERSPECTIVES. THE STRUCTURES ARE COLORED WITH THE STREAM WISE VELOCITY.

tial, denoted as "ring-type" and some cylindrically tubes nearly aligned with the axis, denoted as "cylindrical-type". The "ring-type" vortices are outside the recirculation zone, the "cylindrical-type" showing negative velocities, which means they are inside the inner recirculation zone. Compared to the cold case, the shape of the PVC is more symmetrically and rotates as the cold structure clockwise around the symmetry axis. Nevertheless, a conclusion on the flame stability cannot be drawn.

Even if the modeling approach presented in this study seems to be able to give reasonable results, some limitations of the model should be discussed. First of all, it should be considered, that the adopted reduced mechanism presented in Table 2, does not take the formation of NOx and the interaction between NOx and steam into account. The influence of steam on the obtained results seems to be the increase of the specific heat on the mixture and, therefore, lower peak temperatures.

SUMMARY

Large Eddy Simulations of the non-reacting as well as the reacting field of a swirl-stabilized premix combustor at ultra-wet conditions were performed. The present work used numerical techniques to investigate the flow and coherent structures occurring during vortex break-down. The results were compared with experimental data. The results for the isothermal case were shown to be well in line with the experimental data. Further, the existence of a precessing vortex core could be proofed. The LES provides a full 4D description of the coherent structures leading the way to further detailed studies.

The reactive flow field was investigated using a customized solver for handling low Mach number reacting flows based on an implicit LES approach was developed. As reaction mechanism a reduced 4 steps 7 species global scheme was used. To validate the simulation OH chemiluminescence pictures serve as a reference. The flame spreads further downstream and the main reaction zone is closer to the wall. It was found, that the flame in the simulation was predicted to be too compact. However, the drop-like shape of the main reaction zone is captured. The reduced mechanism recovered the main effects, but a more detailed mechanism would be beneficial. The presence of a PVC could also be determined and was not suppressed by heat-release.

Finally, it was shown that the LES is able to recover the flow field and the large turbulent scales i.e. the source of coherent fluctuations for the non-reacting case. For the reacting case, the LES was able to capture the flame shape and positions satisfactory but the reaction modeling can still be improved.

ACKNOWLEDGMENT

The kind and valuable input of Dr. Robert Szasz is highly appreciated. A part of the computations have been performed at LUNARC (Center for Scientific and Technical Computing at Lund University) and HPC2N facilities within the allocation program SNAC. The research leading to these results has received funding from the European Research Council under the ERC grant agreement n° 247322, GREENEST.

REFERENCES

[1] Lefebvre, A. H., 1995. "The role of fuel-preparation in low-emission combustion". *Journal of Engineering for Gas Turbines and Power,* ***117***, pp. 617–654.

[2] Bhargava, A., Colket, M., Sowa, W., Casleton, K., and Maloney, D., 2000. "An experimental and modeling study of humid air premixed flames". *Journal of Engineering for Gas Turbines and Power,* ***122***, pp. 405–411.

[3] Göke, S., Göckeler, K., Krüger, O., and Paschereit, C. O., 2010. "Computational and experimental study of premixed combustion at ultra wet conditions". In Proceedings of

ASME TURBO EXPO 2010, June 14-18, 2010, Glasgow, Scotland, no. GT2010-23417.

[4] Jonsson, M., and Yan, J., 2005. "Humidified gas turbines - a review of proposed and implemented cycles". *Energy,* ***30***, pp. 1013–1078.

[5] Bianco, M., Camporeale, S. M., and Fortunato, B., 2001. "Cfd simulation of humid air premixed flame combustion chamber for evaporative gas turbine cycles". In Proceedings of ASME TURBO EXPO 2001, no. GT2001-0061.

[6] Guo, P., Zang, S., and Ge, B., 2008. "Les and experimental study of flow features in humid-air combustion chamber with non-premixed circular-disc stabilized flames". In Proceedings of ASME Turbo Expo 2008: Power for Land, Sea and Air, no. GT2008-50940.

[7] Jones, W. P., and Lindstedt, R. P., 1988. "Global reaction schemes for hydrocarbon combustion original research article". *Combustion and Flame,* ***Volume 73***(Issue 3), September, pp. 233–249.

[8] Beer, J. M., and Chigier, N. A., 1974. *Combustion Aerodynamics*. Applied Science Publishers Ltd.

[9] Schneider, C., 2004. *Über die Charakterisierung von Turbulenzstrukturen in verdrallten Strömungen*. VDI-Verlag, Düsseldorf.

[10] Göckeler, K., Göke, S., Schimek, S., and Paschereit, C. O., 2010. "Enhanced recirculation in the cold flow field of a swirl-stabilized burner for ultra wet combustion". In International Conference on Jets, Wakes and Separated Flows.

[11] Jaffe, S., Larjo, J., and Henberg, R., 1991. "Abel inversion using the fast fourier transform". In 10th International Symposium on Plasma Chemistry.

[12] Veynante, D., and Vervisch, L., 2002. "Turbulent combustion modeling". *Progress in Energy and Combustion Science,* ***28***, pp. 193–266.

[13] Weller, H. G., Tabora, G., and Jasak, H., 1998. "A tensorial approach to computational continuum mechanics using object-oriented techniques". *Computers in Physics,* ***12***(6), pp. 620–631.

[14] Smagorinsky, J., 1963. "General circulation experiments with the primitive equations, i. the basic experiment". *Monthly Weather Review,* ***91***(3), March, pp. 99–164.

[15] Issa, R. I., 1986. "Solution of the implicitly discretized fluid flow equations by operator-splitting". *Journal of Computational Physics,* ***62***, pp. 40–65.

[16] Jasak, H., 1996. "Error analysis and estimation for the finite volume method with applications to fluid flows". PhD thesis, Imperial College.

[17] Smith, G. P., Golden, D. M., Frenklach, M., Moriarty, N. W., Eiteneer, B., Goldenberg, M., Bowman, C. T., Hanson, R. K., Song, S., Gardiner, W. C. J., Lissianski, V. V., and Qin, Z., 2000. *GRI 3.0*. `http://www.me.berkeley.edu/gri_mech/`.

[18] Poinsot, T., and Veynante, D., 2001. *Theoretical and Numerical Combustion*. RT Edwards.

[19] Fureby, C., 2007. "Comparison of flamelet and finite rate chemistry les for premixed turbulent combustion". *AIAA Journal,* ***1413***.

[20] Duwig, C., and Fuchs, L., 2008. "Large eddy simulation of a h2/n2 lifted flame in a vitiated co-flow". *Combustion Science and Technology,* ***180***, pp. 453–480.

[21] Grinstein, F. F., and Kailasanath, K., 1994. "Three dimensional numerical simulations of unsteady reactive square jets". *Combustion and Flame,* ***100***, pp. 2–10.

[22] Goldin, G., 2005. "Evaluation of les subgrid reaction models in a lifted flame". *AIAA Journal*, p. 555.

[23] Selle, L., 2004. "Compressible large eddy simulation of turbulent combustion in complex geometry on unstructured meshes". *Combustion and Flame,* ***137***, p. 489505.

[24] Sen, B. A., and Menon, S., 2010. "Linear eddy mixing based tabulation and artificial neural networks for large eddy simulations of turbulent flames". *Combustion and Flame,* ***157***, pp. 62–74.

[25] Duwig, C., and Fuchs, L., 2007. "Study of a confined turbulent jet: influence of combustion and pressure on the flow". *AIAA Journal,* ***vol. 45(3)***, pp. 624–639.

[26] Duwig, C., and Fuchs, L., 2005. "Study of flame stabilization in a swirling combustor using a new flamelet formulation". *Combustion Science and Technology,* ***177***, pp. 1485–1510.

[27] Pitsch, H., and Duchamp de Lageneste, L., 2003. "Large-eddy simulation of premixed turbulent combustion using a level-set approach". *Proceedings of the Combustion Institute,* ***29***, pp. 2001–2008.

[28] Duwig, C., and Fureby, C., 2007. "Large eddy simulation of unsteady lean stratified premixed combustion". *Combustion and Flame,* ***151(12)***, pp. 85–103.

[29] Giacomazzi, E., and Battaglia, V., 2004. "The coupling of turbulence and chemistry in a premixed bluff-body flame as studied by les". *Combustion and Flame,* ***134-4***, pp. 320–335.

[30] Raman, S., and Pitsch, H., 2007. "A consistent les/filtered-density function formulation for the simulation of turbulent flames with detailed chemistry". *Proceedings of the Combustion Institute,* ***31***, pp. 1711–1719.

[31] García-Villalba, M., Fröhlich, J., and Rodi, W., 2006. "Identification and analysis of coherent structures in the near field of a turbulent unconfined annular swirling jet using large eddy simulation". *Physics of Fluids,* ***18***.

[32] Jehong, J., and Hussain, F., 1995. "On the identification of a vortex". *Journal of Fluid Mechanics,* ***285***(69).

[33] Dubief, Y., and Delcayre, F., 2000. "On coherent-vortex identification in turbulence". *Journal of Turbulence,* ***1***(11).

[34] Haller, G., 2005. "An objective definition of a vortex". *Journal of Fluid Mechanics,* ***525***, pp. 1–26.